

Spectral implementation of some quantum algorithms by one- and two-dimensional nuclear magnetic resonance

Ranabir Das[†] and Anil Kumar^{†‡}

[†] *Department of Physics, Indian Institute of Science, Bangalore, India*

[‡] *Sophisticated Instruments Facility, Indian Institute of Science, Bangalore, India*

Quantum information processing has been effectively demonstrated on a small number of qubits by nuclear magnetic resonance. An important subroutine in any computing is the readout of the output. “Spectral implementation” originally suggested by Z.L. Madi, R. Bruschiweiler and R.R. Ernst, [J. Chem. Phys. 109, 10603 (1999)], provides an elegant method of readout with the use of an extra ‘observer’ qubit. At the end of computation, detection of the observer qubit provides the output via the multiplet structure of its spectrum. In “spectral implementation” by two-dimensional experiment the observer qubit retains the memory of input state during computation, thereby providing correlated information on input and output, in the same spectrum. “Spectral implementation” of Grover’s search algorithm, approximate quantum counting, a modified version of Bernstein-Vazirani problem, and Hogg’s algorithm is demonstrated here in three and four-qubit systems.

I. INTRODUCTION

In 1982 Feynmann pointed out that it would be more efficient to simulate the behavior of a quantum system using a quantum, rather than a classical device [1]. The idea of a purpose-built quantum computer which could simulate the physical behavior of a quantum system as well as perform certain tasks much faster than classical computer, attracted immediate attention [2,3]. The theory of such quantum computers is now well understood and several quantum algorithms like Deutsch-Jozsa (DJ) algorithm, Grover’s search algorithm, Shor’s factorization algorithm, Bernstein-Vazirani problem, Hogg’s algorithm and quantum counting have been developed [4–10].

However, building a realistic large scale quantum computer has been extremely challenging [11,12]. Various devices are being examined for building a quantum information processing (QIP) device which is coherent and unitary [11]. Among these, nuclear magnetic resonance (NMR) has shown great promise by demonstrating several quantum algorithms and other QIP tasks on small-scale devices. [13–28]. The last step in any quantum information processing task is the “readout” of the output. Typically in NMR, the readout is obtained by selectively detecting spins [29], or by mapping out the full density matrix [30–32]. It was first pointed out by Ernst et.al. [33] that it is

advantageous from the spectroscopic viewpoint that quantum states can be assigned to individual spectral lines, corresponding to transitions between energy levels rather than to the energy levels themselves [33]. However, for such an advantage one has to use an extra qubit called “observer” qubit. After computation the readout is obtained by detecting only the observer qubit, whose multiplet spectrum provides the result of the computation carried out on the work qubits. Such a “spectral implementation” of a quantum computer was demonstrated by implementation of some logic gates by one- and two-dimensional NMR [33]. Later, “spectral implementation” of a complete set of logic gates and DJ-algorithm [34], Bernstein-Vazirani problem [35] and quantum Fourier transform [36] has also been implemented by NMR. In this work we extend this range by spectrally implementing Grover’s search algorithm, approximate quantum counting, a modified version of Bernstein-Vazirani problem, and Hogg’s algorithm. All the algorithms are implemented by both one- and two-dimensional NMR. To the best of our knowledge this is the first “spectral implementation” of these algorithms.

II. THEORY

A convenient representation of the density matrices of pure states in Liouville space can be obtained by the polarization operators for each qubit (k) [33,37],

$$\begin{aligned}
I_0^k &= |0\rangle\langle 0| = \begin{pmatrix} 1 & 0 \\ 0 & 0 \end{pmatrix} & I_1^k &= |1\rangle\langle 1| = \begin{pmatrix} 0 & 0 \\ 0 & 1 \end{pmatrix} \\
I_+^k &= |0\rangle\langle 1| = \begin{pmatrix} 0 & 1 \\ 0 & 0 \end{pmatrix} & I_-^k &= |1\rangle\langle 0| = \begin{pmatrix} 0 & 0 \\ 1 & 0 \end{pmatrix} \\
I_x^k &= \frac{1}{2}(I_+^k + I_-^k) = \frac{1}{2} \begin{pmatrix} 0 & 1 \\ 1 & 0 \end{pmatrix} & I_y^k &= \frac{1}{2i}(I_+^k - I_-^k) = \frac{1}{2i} \begin{pmatrix} 0 & 1 \\ -1 & 0 \end{pmatrix} \\
I_z^k &= \frac{1}{2}(I_0^k - I_1^k) = \frac{1}{2} \begin{pmatrix} 1 & 0 \\ 0 & -1 \end{pmatrix}
\end{aligned} \tag{1}$$

For example, the density matrix of a pure state $|00\rangle + |11\rangle$ can be expressed as

$$\begin{pmatrix} 1 & 0 & 0 & 1 \\ 0 & 0 & 0 & 0 \\ 0 & 0 & 0 & 0 \\ 1 & 0 & 0 & 1 \end{pmatrix} = |00\rangle\langle 00| + |11\rangle\langle 11| + |00\rangle\langle 11| + |11\rangle\langle 00| \tag{2}$$

$$= I_0^1 I_0^2 + I_1^1 I_1^2 + I_+^1 I_+^2 + I_-^1 I_-^2 \tag{3}$$

The scheme of “spectral implementation” of one-dimensional (1D) and two-dimensional (2D) NMR is respectively given in figure 1(a) and 1(b). We start with the thermal equilibrium density matrix $I_z^0 + I_z^1 + I_z^2 + \dots + I_z^N$ and in the preparation period we create density matrix of the form $I_z^0 I_0^1 I_0^2 \dots I_0^N$, where $I_z^0 I_0^1 I_0^2 \dots I_0^N = (I_0^0 I_0^1 I_0^2 \dots I_0^N - I_0^1 I_0^1 I_0^2 \dots I_0^N)/2$. In this state the last N-1 qubits are simultaneously in pseudopure state (PPS) [13] in two distinct domains of energy levels, in which the observer qubit is in state $|0\rangle$ and $|1\rangle$ respectively. Such a state is known as sub-system pseudopure state [14]. This is further elaborated in figure 2.

The schematic diagram of the energy levels and the spectrum of the observer qubit in a three qubit system, where the first qubit is the observer qubit, is given in figure 2. Figure 2(a) shows the equilibrium deviation populations (populations in excess of uniform background population) of various energy levels and figure 2(b), the equilibrium spectrum of the observer qubit obtained after a $(\pi/2)$ detection pulse. Each of the spectral lines in the multiplet, correspond to the state of the other qubits. The energy level diagram along with the deviation populations after creating the desired initial state of $I_z^0 I_0^1 I_0^2$ is given in 2(c). The corresponding observer qubit spectrum has a single line, that of $|00\rangle$, indicating that the other qubits are in $|00\rangle$ state.

Typically after computation, the density matrix is of the form $I_z^0 I_{0/1}^1 I_{0/1}^2 \dots I_{0/1}^N$, where the subscript 0/1 means that the particular qubit is either in 0 or 1 state. A subsequent $(\pi/2)_y^0$ pulse on the observer (I^0) qubit creates single quantum coherences of the form $I_x^0 I_{0/1}^1 I_{0/1}^2 \dots I_{0/1}^N$, which gives a single line in the spectrum corresponding to the output state of other qubits. An example for the 3-qubit system is given in figure 2. Let us assume that we start with the initial $|00\rangle$ pseudopure state of the qubits (other than observer qubit) and after some computation let the output state be $|11\rangle$. After such a computation, the deviation populations and spectrum of observer qubit are given respectively in figure 2(e) and 2(f).

In some algorithms however, the output is a superposition of multiple states. Then, the output density matrix will have non-zero populations in all the output states and the coherences between them. The spectrum of the observer qubits will thus have multiple lines, corresponding to all the output states. For example, in the 3-qubit system, if the output state of the work qubits is $|00\rangle + |11\rangle$, the density matrix is of the form $I_z^0 I_0^1 I_0^2 + I_z^0 I_1^1 I_1^2 + I_z^0 I_+^1 I_+^2 + I_z^0 I_-^1 I_-^2$. After the $(\pi/2)_y^0$ detection pulse on the observer qubit the single quantum coherences of the terms $I_x^0 I_0^1 I_0^2$ and $I_x^0 I_1^1 I_1^2$ will be detected. The spectrum of the observer qubit will show two lines corresponding to the states of $|00\rangle$

and $|11\rangle$ of the other qubits. The coherences will be converted into multiple quantum coherences which are not detected directly in NMR. Hence, the “spectral implementation” gives a measure of the deviation populations or probabilities of each state but does not measure the coherences, which if required can be measured by state tomography [30–32].

A two-dimensional experiment for “spectral implementation” provides the input and output in the same spectrum. The pulse sequence for the two-dimensional experiment of “spectral implementation” is given in figure 1(b). Suppose a computation starts with the input of $|00..0\rangle$ and end with an output of $|11..1\rangle$ state. After preparation of the initial $I_z^0 I_0^1 I_0^2 .. I_0^N$ state the application of the pulse sequence of figure 1(b) can be analyzed in the following steps:

$$\begin{aligned}
I_z^0 I_0^1 I_0^2 .. I_0^N &\xrightarrow{(\pi/2)_y^0} I_x^0 I_0^1 I_0^2 .. I_0^N \\
&\xrightarrow{t_1} I_x^0 I_0^1 I_0^2 .. I_0^N \cos(\omega_{00..0}^0 t_1) \\
&\xrightarrow{(\pi/2)_{-y}^0, G_z} I_z^0 I_0^1 I_0^2 .. I_0^N \cos(\omega_{00..0}^0 t_1) \\
&\xrightarrow{Comp} I_z^0 I_1^1 I_1^2 .. I_1^N \cos(\omega_{00..0}^0 t_1) \\
&\xrightarrow{(\pi/2)_y^0 - t_2} I_x^0 I_1^1 I_1^2 .. I_1^N \cos(\omega_{00..0}^0 t_1) \cos(\omega_{11..1}^0 t_2), \tag{4}
\end{aligned}$$

where $\omega_{00..0}^0$ and $\omega_{11..1}^0$ are respectively the frequencies of the $|00..0\rangle$ and $|11..1\rangle$ transitions of the observer qubit I^0 , $(\pi/2)_y^0$ is a $(\pi/2)$ rotation of the observer qubit (I^0) about y-axis, G_z is the gradient pulse and $Comp$ is the computation performed on the work qubits. It may be noted that the signal from the observer qubit is modulated by the frequencies corresponding to both the input and the output states of the work qubits. A series of experiments are performed with systematic increment of the t_1 period followed by detection of the observer qubit’s signal. The collected two-dimensional time domain data set $s(t_1, t_2)$ is double Fourier transformed yielding a two-dimensional frequency domain spectrum $S(\omega_1, \omega_2)$, which contains along ω_1 the input states of work qubits before computation and along ω_2 , the output state of work qubits after computation.

III. GROVER’S SEARCH ALGORITHM

Grover’s search algorithm can search an unsorted database of size N in $O(\sqrt{N})$ steps while a classical search would require $O(N)$ steps [5]. Grover’s search algorithm has been earlier demonstrated by NMR [18,19]. The quantum circuit for implementing Grover’s search algorithm on two qubit system

is given in figure 3(a). The algorithm starts from a $|00\rangle$ pseudopure state. A uniform superposition of all states are created by the initial Hadamard gates (H). Then the sign of the searched state “ x ” is inverted by the oracle through the operator

$$U_x = I - 2|x\rangle\langle x|. \quad (5)$$

An inversion about mean is performed on all the states by a diffusion operator $HU_{00}H$, where

$$U_{00} = I - 2|00\rangle\langle 00|. \quad (6)$$

For an N -sized database the algorithm requires $O(\sqrt{N})$ iterations of $U_xHU_{00}H$. For a 2-qubit system with four states, only one iteration is required. We have implemented this algorithm on the two qubits of a three qubit system with the third qubit acting as the observer qubit. The three qubit system chosen for this purpose is 4-fluoro 7-nitro benzofuran (dissolved in CDCl_3), which comprises of a two protons (^1H) and a fluorine (^{19}F). The chemical structure of the molecule along with the equilibrium proton and fluorine spectrum is given in figure 4(a). We have chosen the fluorine spin as the observer qubit. The Hamiltonian of the system is

$$\mathcal{H} = \sum_{i=0}^2 2\pi\nu_i I_z^i + \sum_{i>j} 2\pi J_{ij} I_z^i I_z^j, \quad (7)$$

where ν_i are the resonance frequencies of various spins and J_{ij} are the indirect couplings. The experiments were performed at a field of 11.4 Tesla in a Bruker DRX500 spectrometer. At the magnetic field of 11.4 Tesla, the resonant frequency of proton is 500.13 MHz and that of fluorine is 470.59 MHz. The frequency difference between the two protons is 646 Hz. The J-couplings are $J_{01} = -3.84$ Hz, $J_{02} = 8.01$ Hz and $J_{12} = 8.07$ Hz. The ^1H transmitter frequency is set at the center of the proton spectrum.

The required initial state of $I_z^0|00\rangle\langle 00|$ was prepared by the method of pair of pseudopure states (POPS), originally suggested by Fung [38,39]. The method requires two population distributions, (i) equilibrium populations and (ii) population distribution after a selective (π)-pulse on $|000\rangle \leftrightarrow |100\rangle$. Subtraction of (ii) from (i) effectively gives the initial state of $I_z^0|00\rangle\langle 00|$ (figure 4(b) corresponding to the schematic PPS of figure 2(c)). It might be noted that the method of creation of sub-system pseudopure states from cat-states can also be adopted for creation of this initial state [40].

The Hadamard gates are implemented by $(\pi/2)_{-y}^{1,2}(\pi)_x^{1,2}$ pulse (pulses are applied from left to right) [18], where $(\theta)_x^{1,2}$ denotes a θ -angle pulse (rotation) on 1^{st} and 2^{nd} -qubit about the

x -axis. The U_{00} operator is a controlled phase gate which can be implemented by the sequence $[(\tau/2)(\pi)_x^{1,2}(\tau/2)(\pi)_x^{1,2}][(\pi/2)_{-y}^{1,2}(\pi/2)_{-x}^{1,2}(\pi/2)_y^{1,2}]$, where $\tau = 1/2J_{12}$ [18]. The sequence $[(\tau/2)(\pi)_x^{1,2}(\tau/2)(\pi)_x^{1,2}]$ evolves the system only under the J_{12} -coupling and refocuses all other couplings and proton chemical shifts [37], whereas the $[(\pi/2)_{-y}^{1,2}(\pi/2)_{-x}^{1,2}(\pi/2)_y^{1,2}]$ is a composite z-rotation on both the qubits [41]. Similarly, the other phase gates can be constructed as [18],

$$\begin{aligned} U_{01} &= [(\tau/2)(\pi)_x^{1,2}(\tau/2)(\pi)_x^{1,2}][(\pi/2)_{-y}^{1,2}(\pi/2)_x^1(\pi/2)_{-x}^2(\pi/2)_y^{1,2}] \\ U_{10} &= [(\tau/2)(\pi)_x^{1,2}(\tau/2)(\pi)_x^{1,2}][(\pi/2)_{-y}^{1,2}(\pi/2)_{-x}^1(\pi/2)_x^2(\pi/2)_y^{1,2}] \\ U_{11} &= [(\tau/2)(\pi)_x^{1,2}(\tau/2)(\pi)_x^{1,2}][(\pi/2)_{-y}^{1,2}(\pi/2)_x^{1,2}(\pi/2)_y^{1,2}] \end{aligned} \quad (8)$$

The pulses which are simultaneously applied on both the qubits are achieved by hard pulses. However, some gates require selective excitation of qubits. Since the resonance frequencies of the two protons are relatively close to each other, selective excitation of a particular proton qubit requires long low-power pulses, which introduce significant errors in the computation [17,19]. Fortunately, in case there are two homonuclear qubits, the selective pulses can be substituted by hard pulses and delays using the variation of “jump-and-return” sequence [42], as demonstrated by Jones et.al. [43]. For example, the pulse sequence of U_{01} gate requires $(\pi/2)_x^1(\pi/2)_{-x}^2$ at one point. This can be achieved by using the identity [41]

$$(\pi/2)_{-y}(\pi/2)_{\pm z}(\pi/2)_y = (\pi/2)_{\pm x}. \quad (9)$$

If the proton transmitter frequency is set at the center of the spectrum, then $\nu_1 = -\nu_2 = \nu$, and, a delay of $(1/4\nu)$ evolves the two protons under the Zeeman Hamiltonian of $2\pi\nu(I_z^1 - I_z^2)$ to give the intermediate $(\pi/2)_{\pm z}$ rotation of Eq.[9]. Hence,

$$(\pi/2)_x^1(\pi/2)_{-x}^2 = (\pi/2)_{-y} - (1/4\nu) - (\pi/2)_y. \quad (10)$$

Similarly, the pulse $(\pi/2)_{-x}^1(\pi/2)_x^2$ required for U_{10} gate, can be achieved by

$$(\pi/2)_{-x}^1(\pi/2)_x^2 = (\pi/2)_y - (1/4\nu) - (\pi/2)_{-y} \quad (11)$$

In principle however, the evolution under J-coupling during $(1/4\nu)$ would lead to some non-ideal characteristics [44], which is minimal in our system, since the ratio of maximum J-coupling to chemical shift frequency difference $\sim 1:80$. This error is significantly less than the error introduced due to evolution under internal Hamiltonian during low power long duration qubit selective pulses.

After application of the quantum circuit in figure 3(a) on the initial state of $I_0^z|00\rangle\langle 00|$, the observer qubit was detected by a $(\pi/2)$ pulse. From the obtained spectrum given in figure 5(a), one can identify the searched state ($|x\rangle$) directly. The two-dimensional experiment for “spectral implementation” has the added advantage that the input and output can be identified in a single spectrum. The 2D experiment of figure 1(b) was carried out, where during the computation period, the quantum circuit of figure 3, was implemented on I_1 and I_2 . The resultant spectrum given in figure 5(b), shows the input and output in each case. For example, when $|x\rangle = |11\rangle$, a cross-peak at the frequency of $|00\rangle$ transition along ω_1 to that of the $|11\rangle$ transition along ω_2 , identifies the input as $|00\rangle$ and the output as $|11\rangle$. The 2D spectra in figure 5(b) contains the initial state of $|00\rangle$ and the searched state of $|00\rangle$, $|01\rangle$, $|10\rangle$ and $|11\rangle$. In the 1D spectrum of Fig. 5(a), the initial PPS state has to be ascertained independently prior to the implementation of search algorithm.

IV. APPROXIMATE QUANTUM COUNTING

The search problem may be thought as finding k -entries out of N , which satisfy the condition $f(x) = 1$. For the other, $N - k$ entries, $f(x) = 0$. While Grover’s search algorithm searches these k -items (one at a time), quantum counting finds out the value of k [9,10]. This has extreme importance because in case of multiple solutions, the required number of Grover’s iteration scales as $O(\sqrt{N/k})$ [12]. Hence finding out the number of existing solutions speeds up the search procedure. Moreover, the fact that counting can find out whether the number of solutions is zero or finite, makes it applicable to the non-deterministic (NP)-complete search problems, where it is important to know whether solution exists for a given search problem [12]. Approximate quantum counting has been demonstrated using NMR by Jones and Mosca [43]. In this work we provide a “spectral implementation” of approximate quantum counting in the three qubit system of 4-fluro 7-nitro benzofuran, where the I^2 is the target qubit, I^1 the control qubit and the I^0 , the observed qubit.

The working of counting algorithm, as detailed by Jones and Mosca [43], is as follows. Counting algorithm can be thought of as a method for estimating the eigenvalue of Grover’s iteration $G = HU_0H^{-1}U_f$, where $U_0 = I - 2|00..0\rangle\langle 00..0|$ and U_f transforms $|x\rangle$ to $(-1)^{f(x)+1}|x\rangle$. Starting from the initial $|00..0\rangle$ state, an initial Hadamard on target qubit creates an uniform superposition $H|00..0\rangle = (|\psi_+\rangle + |\psi_-\rangle)/\sqrt{2}$, where $|\psi_+\rangle$ and $|\psi_-\rangle$ are two eigenvectors of G [43]. These two eigen-

vectors are with eigenvalues of $e^{\pm i\phi_k}$, where $\sin(\phi_k/2) = \sqrt{k/N}$. An uniform superposition of the control qubit is also created. The application of controlled G produces the result

$$|\psi_+^1\rangle = (|0\rangle + e^{i\phi_k}|1\rangle)|\psi_+\rangle/\sqrt{2}. \quad (12)$$

If r iterations are performed, then the state is

$$|\psi_+^r\rangle = (|0\rangle + e^{ir\phi_k}|1\rangle)|\psi_+\rangle/\sqrt{2}. \quad (13)$$

A second Hadamard gate on the control qubit produces

$$|\psi_{f+}^r\rangle = [(1 + e^{ir\phi_k})|0\rangle + (1 - e^{ir\phi_k})|1\rangle]|\psi_+\rangle/2. \quad (14)$$

A similar result will happen in the case of $|\psi_-\rangle$. At the end, the final state $|\psi_f\rangle$ will be an entangled state of the control and target qubits, except when $k = 0$ or $k = N$ [9,10,43].

Jones et.al. have implemented the quantum circuit of figure 3(b) in a two-qubit system, measured the signal from control qubit, thereby tracing the target qubit, and shown that the signal assumes a sinusoidal behavior with r whose frequency depend on ϕ_k [43]. We have instead, started from the initial $I_z^0|00\rangle\langle 00|$ state and inferred the result of counting from the spectrum of observer qubit. For a two qubit case only one Grover's iteration is sufficient to get the result [43]. Given in Table 1 are the count k , their corresponding ϕ , the U_f operators and final state of the system for $r = 1$. Note that for $k = 0$, the final state is $|\psi_f\rangle = |00\rangle$ and for $k = N = 2$ the final state is $|\psi_f\rangle = |10\rangle$. For $k = 1$ the output states are in entangled form of all the states, $|00\rangle$, $|01\rangle$, $|10\rangle$ and $|11\rangle$.

Starting with the initial state of $I_z^0|00\rangle\langle 00|$, we implemented the quantum circuit of figure 4(b). The controlled controlled U_0 and controlled $U_{f_{01}}$ have the same operator as that of two-qubit controlled phase gate U_{10} implemented in Grover's algorithm (section II), whose corresponding pulse sequence is given in Eq. [11]. $U_{f_{10}}$ has the same operator and pulse sequence as that of U_{11} in Eq. [11]. $U_{f_{11}}$ is an identity operator and required no pulses. $U_{f_{00}}$ required a $(\pi)_z^1$ rotation. This $(\pi)_z^1$ rotation was implemented with hard pulses and evolution under Zeeman Hamiltonian,

$$(\pi)_z^1 = (1/4\nu) - [(\pi/2)_{-y}^{1,2}(\pi/2)_x^{1,2}(\pi/2)_y^{1,2}]. \quad (15)$$

During the delay $(1/4\nu)$ the system evolves under the Zeeman Hamiltonian to acquire a rotation of $(\pi/2)_z^1(\pi/2)_{-z}^2$. The subsequent composite z-pulse was applied on both qubits, $(\pi/2)_z^{1,2} = [(\pi/2)_{-y}^{1,2}(\pi/2)_x^{1,2}(\pi/2)_y^{1,2}]$, which cancels the rotation of second qubit but adds to the rotation of first

qubit to give an effective $(\pi/2)_z^1$ rotation. It may be noticed that there are two pseudo-Hadamard gates on second qubit which require spin-selective pulses since $h=(\pi/2)_y$ and $h^{-1}=(\pi/2)_{-y}$. However, these pulses can also be performed by hard pulses and evolution under Zeeman Hamiltonian using the "jump-and-return" logic [43].

$$\begin{aligned}(\pi/2)_y^2 &= (\pi/2)_x^{1,2} - (1/8\nu) - (\pi/2)_{-x}^{1,2}(\pi/4)_y^{1,2}, \\(\pi/2)_{-y}^2 &= (\pi/2)_{-x}^{1,2} - (1/8\nu) - (\pi/2)_x^{1,2}(\pi/4)_{-y}^{1,2}.\end{aligned}\tag{16}$$

After implementing the quantum circuit of figure 3(b), the observer qubit was measured. The observer qubit's spectrum given in figure 6(a), shows four lines for $k = 1$ (f_{01} and f_{10}). For $k = 0$ (f_{00}), only $|00\rangle$ transition and for $k = 2$ (f_{11}), only $|10\rangle$ transition is observed. The 2D-spectrum of figure 6(b) contains correlation of the output state with the initial $|00\rangle$ pseudopure state, and confirms the same result.

V. BERSTEIN-VAZIRANI PROBLEM

Berstein and Vazirani considered the problem of determining a n-bit string "a" [8]. Classically each query would yield one bit of information and hence would require n-queries to the database. However, Bernstein and Vazirani showed that a quantum algorithm can solve the problem with one quantum query [8]. For this purpose, the oracle has to compute a function $f_a(x) = a.x$. The scheme proposed by Bernstein and Vazirani required an ancillary qubit and determined a n-qubit string with n+1 qubits, which has been demonstrated by NMR recently [36]. However, Du and his co-workers had simplified the scheme such that the ancillary qubit was not required [46]. We have implemented the Du-scheme, since it has the advantage of determining a n-qubit string with n-qubit system. The quantum circuit of a two-qubit implementation is given in figure 3(c). Starting from $|0\rangle^n$, the Hadamard gates create an uniform superposition

$$|\psi_1\rangle = \frac{1}{2^{n/2}} \sum_{x=0}^{2^n-1} |x\rangle\tag{17}$$

The U_a operator transforms $|x\rangle \rightarrow (-1)^{f_a(x)}|x\rangle$. The unitary operator U_a can be decomposed into direct products of single-qubit operations [46]

$$U_a = U^1 \otimes U^2 \otimes \dots \otimes U^n,$$

$$\begin{aligned}
U^i &= I, & a_i &= 0 \\
&= \sigma_z, & a_i &= 1 \\
I &= \begin{pmatrix} 1 & 0 \\ 0 & 1 \end{pmatrix}, & \sigma_z &= \begin{pmatrix} 1 & 0 \\ 0 & -1 \end{pmatrix}
\end{aligned} \tag{18}$$

Operation of U_a creates a new state $|\psi_2\rangle$ of the form,

$$|\psi_2\rangle = U_a|\psi_1\rangle = \frac{1}{2^{n/2}} \sum_{x=0}^{2^n-1} (-1)^{a \cdot x} |x\rangle. \tag{19}$$

The final state after the subsequent Hadamard operation is

$$|\psi_3\rangle = H|\psi_2\rangle = \frac{1}{2^n} \sum_{x=0}^{2^n-1} \sum_{y=0}^{2^n-1} (-1)^{a \cdot x} (-1)^{x \cdot y} |y\rangle \tag{20}$$

However, since $\sum_{x=0}^{2^n-1} (-1)^{a \cdot x} (-1)^{x \cdot y} = \delta_{a,y}$ [2], $|\psi_3\rangle = |a\rangle$ [8,43].

The algorithm was implemented to determine a two-qubit string by ‘‘spectral implementation’’ using three qubit system of 4-fluro 7-nitro benzofuran. After creating POPS, followed by Hadamard pulses, the operator U_a was applied for $|a\rangle = |00\rangle, |01\rangle, |10\rangle$ and $|11\rangle$. U_{00} is unity operator and does not require any pulse. U_{10} is σ_z^1 , which requires a $(\pi)_z^1$ rotation. Once again, the $(\pi)_z^1$ rotation was implemented using the pulse sequence of Eq.[15]. Similarly, U_{01} was implemented by

$$(\pi)_z^2 = (\pi)_x^{1,2}(1/4\nu)(\pi)_x^{1,2} - [(\pi/2)_{-y}^{1,2}(\pi/2)_x^{1,2}(\pi/2)_y^{1,2}]. \tag{21}$$

U_{11} is $\sigma_z^1\sigma_z^2$, which can be achieved by a composite z-pulse of $(\pi)_z^{1,2} = (\pi/2)_{-y}^{1,2}(\pi)_x^{1,2}(\pi/2)_y^{1,2}$. After application of the final Hadamard pulses, the observer qubit was detection by a $(\pi/2)$ pulse. The obtained spectrum given in figure 7(a), clearly determines the 2-bit string in each case. The result of 2D experiment is given in figure 7(b). The 2D spectrum correlates the input $|00\rangle$ to the output in each case.

The above algorithm was also implemented to determine a three-qubit string by ‘‘spectral implementation’’ using a four-qubit system. The molecule 2-3 difluoro 6-nitrophenol (dissolved in CDCl_3+1 drop D_2O) has 4 weakly coupled spin-1/2 nuclei. The proton of the phenol group is exchanged with the D_2O . The two remaining protons and the two fluorine nuclei constitute the four-qubit system. The equilibrium spectrum of each nucleus is given in Fig. 8 (a). In a 500 MHz NMR spectrometer, the chemical shift difference between the two Fluorine spins is 16 kHz while that between the two protons is 560 Hz. The couplings range from 19.13 Hz to -2.4 Hz.

The operators and pulse sequences required for each string of a three qubit system is given in Table 2. Since the chemical shift difference between the two fluorine spins are considerably large (16kHz), selective pulses do not introduce significant errors. The pulses on fluorine spin I^3 were achieved by Gaussian shaped selective pulses of $12.5\mu\text{s}$ duration. The proton transmitter frequency was kept at the middle of the spectrum and the selective z-pulses on protons were applied in similar logic as in the two-qubit case (Eq. [15] and [21]). Hard pulses were applied when both protons had to be pulsed simultaneously. The algorithm was implemented starting from the initial state of $I_z^0|000\rangle\langle 000|$ (figure 8(b)) and finally the observed qubit was measured by selective Gaussian shaped $(\pi/2)_y$ pulse. The only transition present in each spectrum given in figure 9(a) indicates the corresponding string. The 2D experimental spectra given in figure 9(b) verify the same results, correlating the input state of $|000\rangle$ in each case.

VI. HOGG'S ALGORITHM

Satisfiability (SAT) problem is one of the nondeterministic polynomial (NP) combinatorial search problems [7]. SAT problem consists of a logical formula in n variables, V_1, V_2, \dots, V_n [7]. One has to find an assignment (true or false) for each variable V_i , such that it makes the formula true. The logical formula can be expressed in various equivalent forms, as conjunction of clauses, where a clause is a disjunction of some variables. A clause with k variables is false for exactly one set of values for its variables but true for the other $2^k - 1$ sets. An example of clause for $k=3$ is $V_1 \text{ OR } V_2 \text{ OR } V_3$, where the clause is *false* for only $V_1 = V_2 = V_3 = \textit{false}$. Only the assignments which satisfy all the clauses are considered as solutions [7].

While the number of steps required by a classical algorithm increase linearly with the size of the variables [7], Hogg's algorithm can solve 1-SAT and maximally constrained k -SAT problems in a single step, whatever be the size of the variable [7]. Hogg's algorithm has been successfully implemented by NMR in a three qubit system [45]. Here we demonstrate Hogg's algorithm by "spectral implementation". The Hogg's algorithm starts by creating a uniform superposition of states by initializing from $|\psi_0\rangle = |0\rangle^{\otimes n}$ and applying Hadamard gate on all qubits $|\psi_1\rangle = H^{\otimes n}|\psi_0\rangle = 2^{-n/2} \sum_s |s\rangle$. Let m be the number of clauses in the 1-SAT logical formula. Then the unitary operations UR are consecutively applied to yield the final state $|\psi_f\rangle = UR|\psi_1\rangle$ where U and R

defined as follows. R adjusts the phases of $|s\rangle$ depending on the conflicts c of the different assignments in the superposition of s , ranging from 0 to m . R is a diagonal matrix of the form

$$\begin{aligned} R^{ss} &= \sqrt{2}\cos[(2c-1)\pi/4], & \text{for even } m \\ &= i^c & \text{for odd } m \end{aligned} \quad (22)$$

The operator U mixes the amplitudes from different assignments with elements U_{rs} , depending the Hamming distance d between r and s . U is of the form

$$\begin{aligned} U_{rs} &= U_{d(r,s)} \\ &= 2^{-(n-1)/2}\cos[(n-m+1-2d)\pi/4] & \text{for even } m \\ &= 2^{-n/2}e^{i\pi(n-m)/4}(-i)^d & \text{for odd } m \end{aligned} \quad (23)$$

where $d = |r| + |s| - |r \wedge s|$ is the Hamming distance between r and s , i.e. number of positions at which their values differ. U can be decomposed into $H\Gamma H$ where H is the Hadamard matrix and Γ is a diagonal matrix of the form

$$\begin{aligned} \Gamma_{rr} = \gamma(r) = \gamma_h &= \sqrt{2}\cos[(m-2h-1)\pi/4] & \text{for even } m \\ &= i^h e^{-i\pi m/4} & \text{for odd } m \end{aligned} \quad (24)$$

where $h = |r|$, and hence Γ_{rr} depend on the number of 1-bits in each assignment. For a detailed description of the working of the algorithm see ref [7]. Hence the Hogg's quantum starts with the initial $|00\rangle$ state and reaches the desired output state $|\psi_f\rangle$ by

$$|\psi_f\rangle = URH|00\rangle \quad (25)$$

and the final step is to measure the output state $|\psi_f\rangle$. We have observed the final state through detection of the observer qubit.

The quantum circuit of Hogg's algorithm for a three-qubit system is given in figure 3(d). While implementing the corresponding pulse sequence, the consecutive pulses of opposite phases cancel out, yielding a simplified sequence [45]. The $m = 1$ and 3 clauses, their logic formulae and the reduced pulse sequences are given in table 3 [45]. Only the $m=1$ and 3 cases are demonstrated here for ease of implementation. The selective pulses on fluorine spin were achieved using Gaussian shaped pulses. In protons, the selective pulses were achieved by hard pulses concatenated with Zeeman evolution (Eq. [10], [11] and [16]). For example, while implementing V_1 ,

$$\begin{aligned}
V_1 : [(\pi)_x^1][(\pi/2)_y^2][(\pi/2)_y^3] &= [(\pi/2)_{-y}^{1,2} - 1/4\nu - (\pi/2)_y^{1,2}(\pi/2)_x^{1,2}] \\
&\quad [(\pi/2)_{-x}^{1,2} - 1/8\nu - (\pi/2)_x^{1,2}(\pi/4)_y^{1,2}][(\pi/2)_y^3] \\
&= [(\pi/2)_{-y}^{1,2} - 1/4\nu - (\pi/2)_y^{1,2} - 1/8\nu - (\pi/2)_x^{1,2}(\pi/4)_y^{1,2}][(\pi/2)_y^3] \quad (26)
\end{aligned}$$

The spectra obtained by the one-dimensional experiment is given in figure 10 while the spectra obtained in 2D-experiment is given in figure 11. The spectra of observer qubit clearly identifies the desired outputs of table 3. For example, in the case of V_1 , the output has all the states that satisfy the condition that 1st qubit is $|1\rangle$ or *false*; namely $|001\rangle$, $|011\rangle$, $|101\rangle$ and $|111\rangle$ (read the order of qubits from right to left). Similarly, for $V_3 \wedge V_2 \wedge V_1$, the output consists of the sole answer $|111\rangle$, which satisfies the condition that all the qubits are in state $|1\rangle$.

VII. CONCLUSION

We have demonstrated “spectral implementation” of several quantum algorithms by one- and two-dimensional NMR. Provided future quantum computers run with high fidelity, “spectral implementation” delivers an aphoristic method of readout. Though it requires the use of an observer qubit, this qubit also helps in creating a pseudopure state by non-scalable and effective methods like POPS [38]. With the essentiality that the observer qubit has resolved spectrum, the principle of “spectral implementation” is applicable to higher qubit systems without increasing complexity.

VIII. ACKNOWLEDGMENT

Useful discussions with Prof. G. S. Agarwal are gratefully acknowledged. The use of DRX-500 NMR spectrometer funded by the Department of Science and Technology (DST), New Delhi, at the Sophisticated Instruments Facility, Indian Institute of Science, Bangalore, is also gratefully acknowledged. AK acknowledges ”DAE-BRNS” for the award of ”Senior Scientists scheme” and DST for a research grant for ”Quantum Computing by NMR”.

[1] R.P. Feynman, Int J. Theor. Phys. **21**, (1982) 467.

- [2] J. Preskill, *Lecture notes for Physics 229: Quantum information and Computation*, <http://theory.caltech.edu/people/preskill/>.
- [3] S. Lloyd, *Science* **273**, 1073 (1996).
- [4] D. Deutsch and R. Jozsa, *Proc. R. Soc. Lond. A* **400**, 97 (1985).
- [5] L.K. Grover, *Phys. Rev. Lett.* **79**, (1997) 325.
- [6] P.W.Shor, *SIAM Rev.* **41**, 303-332 (1999).
- [7] T. Hogg. *Phys. Rev. Lett.* **80**, 2473 (1998).
- [8] E. Bernstein and U. Vazirani, *SIAM J. Computin.* **26**, 1411 (1997).
- [9] M. Boyer, G. Brassard, P. Hoyer, and A. Tapp. *Fortschr. Phys.* **46**, 493 (1998).
- [10] G. Brassard, P Hoyer and A. Tapp, in *Automata, Languages, and Programming: Proceedings of the 25th International Colloquium, ICALP'98, Aalborg, Denmark, 1998* (Springer, Berlin, 197); quant-ph/9805082.
- [11] D. Bouwmeester, A. Ekert and A. Zeilinger, (Ed) *The Physics of Quantum Information*, Springer, 2000.
- [12] M.A. Nielsen and I.L. Chuang, *Quantum Computation and Quantum Information*, Cambridge University Press 2000.
- [13] D. G. Cory, A.F. Fahmy and T.F. Havel, *Proc.Natl.Acad.Sci. USA* **94**, 1634 (1997).
- [14] N. Gershenfeld and I.L. Chuang, *Science* **275**, 350 (1997).
- [15] D. G. Cory, M. D. Price and T.F. Havel, *Physica D*, **120**, 82 (1998).
- [16] I. L.Chuang, L. M. K. Vanderspyen, X. Zhou, D.W. Leung, and S. Llyod, *Nature (London)* **393**, 1443 (1998).
- [17] J. A. Jones and M. Mosca, *J. Chem. Phys.* **109**, 1648 (1998).
- [18] I. L. Chuang, N. Gershenfeld, and M. Kubinec, *Phys. Rev. Lett.* **80**, 3408-3411 (1998).
- [19] J. A. Jones, M. Mosca and R. H. Hansen, *Nature* **393** 344 (1998).
- [20] Kavita Dorai, T. S. Mahesh, Arvind and Anil Kumar, *Current Science*, **79** (10) 1447 (2000).
- [21] Kavita Dorai, Arvind, Anil Kumar, *Phys Rev A.* **61**, 042306 (2000).
- [22] N. Sinha, T.S. Mahesh, K.V. Ramanathan and Anil Kumar, *J. Chem. Phys.* **114**, 4415 (2001).
- [23] Arvind, K. Dorai and Anil Kumar, *Pramana* **56** 7705 (2001).
- [24] L.M.K. Vanderspyen, Matthias Steffen, Gregory Breyta, C.S.Yannoni, M.H. Sherwood and I.L. Chuang, *Nature* **414**, 883 (2001).
- [25] Anil Kumar, K. V. Ramanathan, T. S. Mahesh, N. Sinha and K.V.R.M. Murali, *Pramana* **59** 243 (2002).

- [26] Ranabir Das and Anil Kumar, Phys. Rev. A. **68**, 032304 (2003).
- [27] Ranabir Das, A. Mitra, S. Vijaykumar and Anil Kumar Int. Jour. of Quant. Infor. 1(3) 387 (2003).
- [28] Ranabir Das, Sukhendu Chakraborty, K. Rukmani and Anil Kumar, Phys. Rev. A. (in press).
- [29] J. A. Jones, chapter 5, page 181 of reference [11].
- [30] I.L. Chuang, N. Greshenfeld, M.Kubinec, and D. Leung, Proc. R. Soc. Lond. A **454**, 447 (1998).
- [31] Ranabir Das, T.S. Mahesh and Anil Kumar, Phys. Rev. A. **67**, 062304 (2003).
- [32] Garrett M. Leskowitz and Leonard J. Mueller, Phys. Rev. A. **69**052302 (2004).
- [33] Z.L. Madi, R. Bruschiweiler and R.R. Ernst, J. Chem. Phys. **109**, 10603 (1998).
- [34] T. S. Mahesh, Kavita Dorai, Arvind, Anil Kumar, J. Mag. Res. **148**, 95 (2001).
- [35] X. Peng, X. Zhu, X. Fang, M. Feng, X. Yang, M. Liu, and K. Gao, quant-ph/0202010.
- [36] X. Peng, X. Zhu, X. Fang, M. Feng, M. Liu, and K. Gao, *J. Chem. Phys.* **120**, 3579 (2004).
- [37] R.R. Eersnt, G. Bodenhausen, and A. Wokaun, *Principles of Nuclear Magnetic Resonance in One and Two Dimensions*, Oxford university press 1987.
- [38] B. M. Fung, Phys. Rev. A **63**, 022304 (2001).
- [39] Vladimir L. Ermakov and B. M. Fung, J. Chem. Phys. **118**, 10376 (2003).
- [40] E. Knill, R. Laflamme, R. Martinez, and C.-H. Tseng, Nature (London) 404, 368 (2000).
- [41] R. Freeman, T.A. Frenkiel and M.H. Levitt, *J. Mag. Res.***44**, 409(1981).
- [42] P. Plateau and M. Guron, J. Am. Chem. Soc. **104**, 7310 (1982).
- [43] J. A. Jones amd M. Mosca, Phys. Rev. Lett. **83** 1050 (1999).
- [44] H. K. Cummins C. Jones A. Furze, N. F. Soffe, M. Mosca, J. M. Peach and J. A. Jones, Phys. Rev. Lett **88** 187901 (2002).
- [45] X. Peng, X. Zhu, X. Fang, M. Feng, M. Liu, and K. Gao, Phys. Rev. A. **65** 042315 (2002).
- [46] J. Du, M. Shi, X. Zhou, Y. Fan, B. Ye, and R. Han, Phys. Rev. A. **64** 042306 (2001).

Table 1 :The various possible the count k for a two-qubit system, their corresponding ϕ , the U_f operators and final state of the system $|\psi_{output}\rangle$.

k	ϕ_k	U_f	$ \psi_{output}\rangle$
0	0	$U_{f_{00}} = \begin{pmatrix} 1 & 0 & 0 & 0 \\ 0 & 1 & 0 & 0 \\ 0 & 0 & -1 & 0 \\ 0 & 0 & 0 & -1 \end{pmatrix}$	$ 00\rangle$
1	$\pi/2$	$U_{f_{01}} = \begin{pmatrix} 1 & 0 & 0 & 0 \\ 0 & 1 & 0 & 0 \\ 0 & 0 & -1 & 0 \\ 0 & 0 & 0 & 1 \end{pmatrix}$	$ 00\rangle - 01\rangle + 10\rangle + 11\rangle$
1	$\pi/2$	$U_{f_{10}} = \begin{pmatrix} 1 & 0 & 0 & 0 \\ 0 & 1 & 0 & 0 \\ 0 & 0 & 1 & 0 \\ 0 & 0 & 0 & -1 \end{pmatrix}$	$ 00\rangle + 01\rangle + 10\rangle - 11\rangle$
2	π	$U_{f_{11}} = \begin{pmatrix} 1 & 0 & 0 & 0 \\ 0 & 1 & 0 & 0 \\ 0 & 0 & 1 & 0 \\ 0 & 0 & 0 & 1 \end{pmatrix}$	$ 10\rangle$

Table 2: The operators and pulse sequences required for determination of each string in a three qubit system

string	Operator	Pulse sequence
$ 000\rangle$	I	no pulse
$ 001\rangle$	σ_z^3	$(\pi)_z^3$
$ 010\rangle$	σ_z^2	$(\pi)_z^2$
$ 011\rangle$	$\sigma_z^2\sigma_z^3$	$(\pi)_z^2(\pi)_z^3$
$ 100\rangle$	σ_z^1	$(\pi)_z^1$
$ 101\rangle$	$\sigma_z^1\sigma_z^3$	$(\pi)_z^1(\pi)_z^3$
$ 110\rangle$	$\sigma_z^1\sigma_z^2$	$(\pi)_z^{1,2}$
$ 111\rangle$	$\sigma_z^1\sigma_z^2\sigma_z^3$	$(\pi)_z^{1,2}(\pi)_z^3$

Table 3: Logic formulae for $m=1$ or $m=3$ in a 3-qubit system, corresponding pulse sequences, and theoretical solutions [45]. Read the order of qubits from right to left.

m	Logic formula	Reduced pulse sequence	Final state $ \psi_f\rangle$
1	V_1	$(\pi)_x^1(\pi/2)_y^2(\pi/2)_y^3$	$ 001\rangle + 011\rangle + 101\rangle + 111\rangle$
	\bar{V}_1	$(\pi/2)_y^2(\pi/2)_y^3$	$ 000\rangle + 010\rangle + 100\rangle + 110\rangle$
	V_2	$(\pi/2)_y^1(\pi)_x^2(\pi/2)_y^3$	$ 010\rangle + 011\rangle + 110\rangle + 111\rangle$
	\bar{V}_2	$(\pi/2)_y^1(\pi/2)_y^3$	$ 000\rangle + 001\rangle + 100\rangle + 101\rangle$
	V_3	$(\pi/2)_y^1(\pi/2)_y^2(\pi)_x^3$	$ 100\rangle + 101\rangle + 110\rangle + 111\rangle$
	\bar{V}_3	$(\pi/2)_y^1(\pi/2)_y^2$	$ 000\rangle + 001\rangle + 010\rangle + 011\rangle$
3	$V_3 \wedge V_2 \wedge V_1$	$(\pi/2)_x^{1,2,3}(\pi/2)_{-y}^{1,2,3}(\pi/2)_x^{1,2,3}$	$ 111\rangle$
	$V_3 \wedge V_2 \wedge \bar{V}_1$	$(\pi/2)_{-x}^1(\pi/2)_x^{2,3}(\pi/2)_{-y}^{1,2,3}(\pi/2)_x^{1,2,3}$	$ 110\rangle$
	$V_3 \wedge \bar{V}_2 \wedge V_1$	$(\pi/2)_x^{1,3}(\pi/2)_{-x}^2(\pi/2)_{-y}^{1,2,3}(\pi/2)_x^{1,2,3}$	$ 101\rangle$
	$V_3 \wedge \bar{V}_2 \wedge \bar{V}_1$	$(\pi/2)_{-x}^{1,2}(\pi/2)_x^3(\pi/2)_{-y}^{1,2,3}(\pi/2)_x^{1,2,3}$	$ 100\rangle$
	$\bar{V}_3 \wedge V_2 \wedge V_1$	$(\pi/2)_x^{1,2}(\pi/2)_{-x}^3(\pi/2)_{-y}^{1,2,3}(\pi/2)_x^{1,2,3}$	$ 011\rangle$
	$\bar{V}_3 \wedge V_2 \wedge \bar{V}_1$	$(\pi/2)_{-x}^{1,3}(\pi/2)_x^2(\pi/2)_{-y}^{1,2,3}(\pi/2)_x^{1,2,3}$	$ 010\rangle$
	$\bar{V}_3 \wedge \bar{V}_2 \wedge V_1$	$(\pi/2)_x^1(\pi/2)_{-x}^{2,3}(\pi/2)_{-y}^{1,2,3}(\pi/2)_x^{1,2,3}$	$ 001\rangle$
	$\bar{V}_3 \wedge \bar{V}_2 \wedge \bar{V}_1$	$(\pi/2)_{-x}^{1,2,3}(\pi/2)_{-y}^{1,2,3}(\pi/2)_x^{1,2,3}$	$ 000\rangle$

Figure Captions

Figure 1. Experimental protocol for “spectral implementation” of quantum algorithms [33]. (a) One-dimensional experiment. The first stage is to create an subsystem pseudopure state of the type $I_z^0 I_0^1 I_0^2 \dots I_0^N$, followed by computation on $I^1 \dots I^N$ qubits. Finally the transitions of the observer qubit I^0 are detected by a 90_y° pulse. (b) Two-dimensional experiment. After the creation of initial $I_z^0 I_0^1 I_0^2 \dots I_0^N$ subsystem PPS, the observer qubit is flipped by 90_y° pulse to transverse magnetization and allowed to evolve for a time t_1 . During t_1 , the transitions of the observer qubit modulate with the frequencies characterized by the input state of the other N qubits. A subsequent 90_{-y}° brings the magnetization back to longitudinal direction. The computation is performed on the $I^1 \dots I^N$ qubits. The transitions of the observer qubit are finally detected by a 90_y° pulse. A series of experiments are performed with systematic increment of the t_1 period and the collected 2D data set $s(t_1, t_2)$ is Fourier transformed to get the 2D spectrum $S(\omega_1, \omega_2)$.

Figure 2. Schematic diagram of the energy levels and the spectrum of the observer qubit at different stages of “spectral implementation”. (a) Deviation equilibrium populations. The dotted arrows denote the transitions of observer qubit. (b) Equilibrium spectrum of observer qubit shown by stick diagram. Each transition of the spectrum correspond to the state of other qubits, which are given above each line. (c) Deviation populations after creation of $|00\rangle$ subsystem pseudopure state by POPS. Populations of only $|00\rangle$ eigenstate is non-zero in the two distinct domains of energy levels, where observer qubit is respectively in state $|0\rangle$ and $|1\rangle$. (d) Spectrum of observer qubit after creation of POPS. The dots denote null intensity. (e) Deviation populations after a typical computation whose output is $|11\rangle$. (f) Spectrum of observer qubit after such a computation.

Figure 3. The quantum circuits of various algorithms. (a) Quantum circuit for implementation of Grover’s search algorithm in a 2-qubit system. (b) Quantum circuit for implementation of approximate quantum counting in a 2-qubit system. (c) Quantum circuit for implementation of Bernstein-Vazirani problem. (d) Quantum circuit for implementation of Hogg’s algorithm in a 3-qubit system.

Figure 4. (a) Chemical structure and equilibrium spectrum of 4-fluro 7-nitro benzofuran. The J-coupling values are $J_{01} = -3.84$ Hz, $J_{02} = 8.01$ Hz and $J_{12} = 8.07$ Hz. The peak denoted by asterisk (*) belongs to solvent. (b) Spectra after creation of POPS. A Gaussian shaped selective pulse of 500ms duration was applied on the $|000\rangle \leftrightarrow |100\rangle$ transition and the resultant spectra is subtracted

from the equilibrium spectra of figure (a) to yield (b). [See figure 2(c)]

Figure 5. (a) “Spectral implementation” of Grover’s search algorithm by 1D experiment. After computation, the observer qubit is detected by a non-selective pulse of $14 \mu s$. 4×1024 data points were collected and zero-filled to 8×1024 before Fourier transform. The observer qubit’s spectra shows only the transition corresponding to the searched state ($|x\rangle$) with non-zero intensity. (b) “spectral implementation” of Grover’s search algorithm by 2D experiment. A 2D data set of 256×16 ($t_2 \times t_1$) was collected and zero-filled to 1024×256 . It may be noticed that the total size of the raw 2D dataset is of the same size as that of the 1D experiment. The doubly Fourier transformed spectra gives the input state along ω_1 and output state along ω_2 .

Figure 6. (a) “Spectral implementation” of approximate quantum counting by 1D experiment. 4×1024 data points were collected and zero-filled to 8×1024 before Fourier transform. The observer qubit’s spectra show the transitions corresponding to the output state. Hence the various cases of $k=0$ (f_{00}), $k=1$ (f_{01} and f_{10}), and $k=2$ (f_{11}) can be easily identified from the spectra. (b) “spectral implementation” of approximate quantum counting by 2D experiment. A 2D data set of 256×16 ($t_2 \times t_1$) was collected and zero-filled to 1024×256 . The Fourier transformed spectra gives the output state as well as the input state.

Figure 7. (a) “Spectral implementation” of Bernstein-Vazirani problem in a 2-qubit system. The observer qubit’s spectra shows the transitions corresponding to the bit string. The strings $a = 00$, $a = 01$, $a = 10$ and $a = 11$ can be identified directly from the spectra. (b) 2D “spectral implementation” of Bernstein-Vazirani problem. A 2D data set of 256×16 ($t_2 \times t_1$) was collected and zero-filled to 1024×256 before Fourier transform. The Fourier transformed spectra gives the bit string against the input state in each case.

Figure 8. (a) Chemical structure and equilibrium spectrum of 4-fluoro 7-nitro benzofuran. The J-coupling values are $J_{01} = 5.23$ Hz, $J_{02} = 8.85$ Hz, $J_{03} = 19.1$ Hz, $J_{12} = 9.76$ Hz, $J_{13} = -2.4$ Hz and $J_{23} = 6.81$ Hz. (b) Spectra after creation of POPS. A Gaussian shaped selective pulse of 500ms duration was applied on the $|0000\rangle \leftrightarrow |1000\rangle$ transition and the resultant spectra is subtracted from the equilibrium spectra of figure (a) to yield (b).

Figure 9. (a) “Spectral implementation” of Bernstein-Vazirani problem in a 3-qubit system. After computation, the observer qubit is detected by a selective pulse of 12.5us duration. The observer qubit’s spectra show the transitions corresponding to the bit string. The eight possible strings of $a =$

000, $a = 001 \dots a = 111$ can be identified directly from the spectra. (b) 2D “spectral implementation” of Bernstein-Vazirani problem in the three-qubit case. A 2D data set of 256×24 ($t_2 \times t_1$) was collected and zero-filled to 1024×256 before Fourier transform. The Fourier transformed spectra give the various bit strings along with the input state in each case.

Figure 10. One-dimensional “spectral implementation” of Hogg’s algorithm in a 3-qubit system. After computation, the observer qubit is detected by a selective pulse of $12.5 \mu s$ duration. The observer qubits spectra clearly show the output states corresponding to various logical formulae of table 3. (a) contains the spectra corresponding to $m=1$ and (b) to $m=3$.

Figure 11. Two-dimensional “spectral implementation” of Hogg’s algorithm in a 3-qubit system. The two-dimensional spectra provides the output states corresponding to various logical formulae of table 3. (a) contains the spectra corresponding to $m=1$ and (b) to $m=3$.

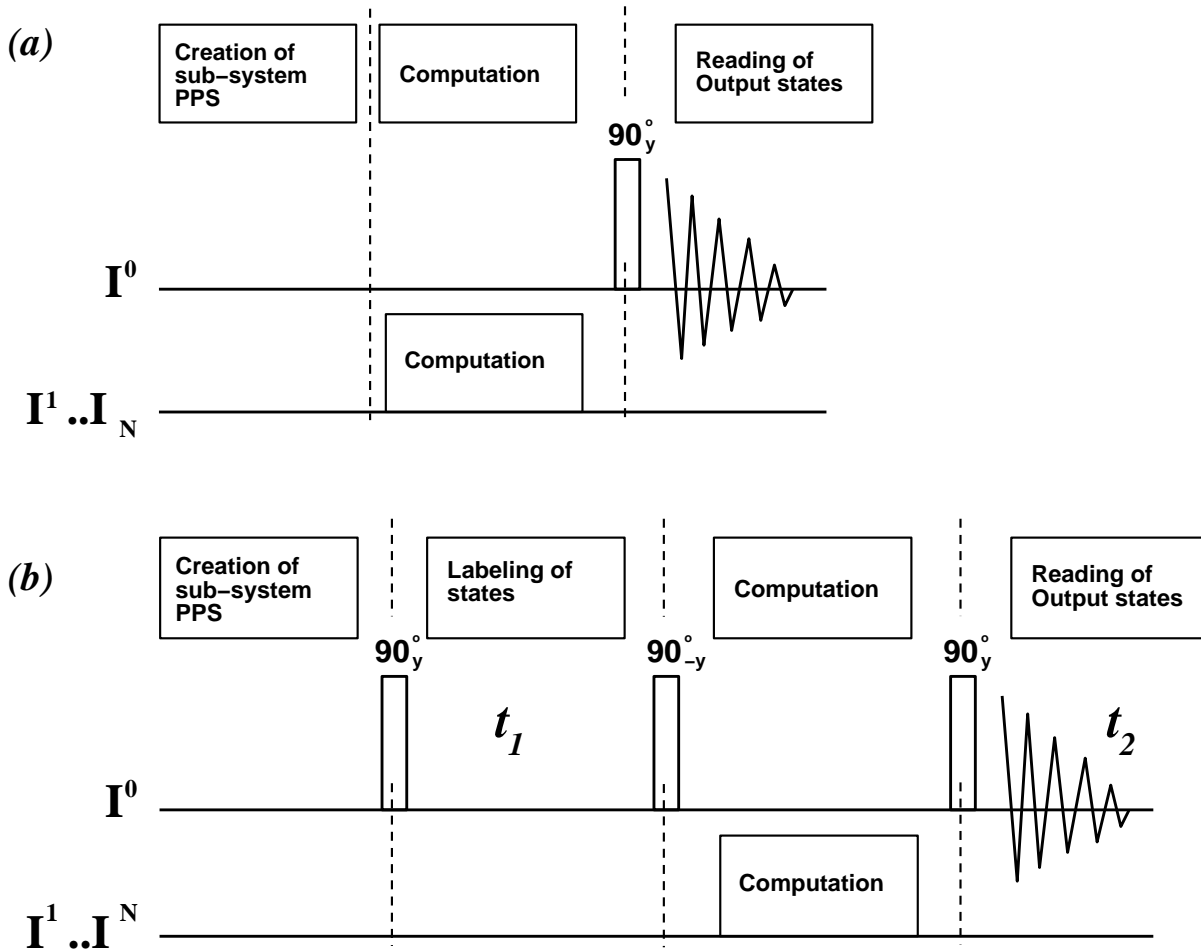


Figure 1

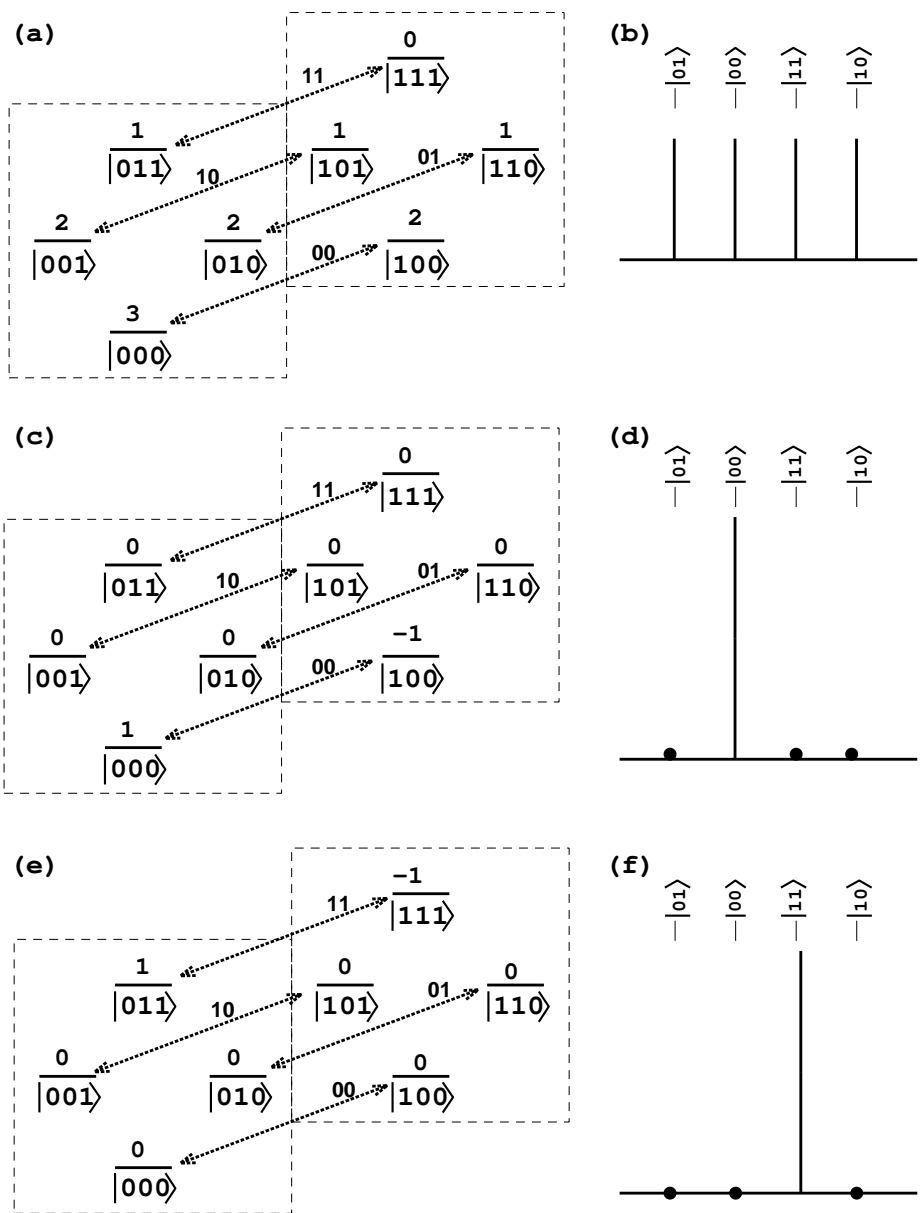
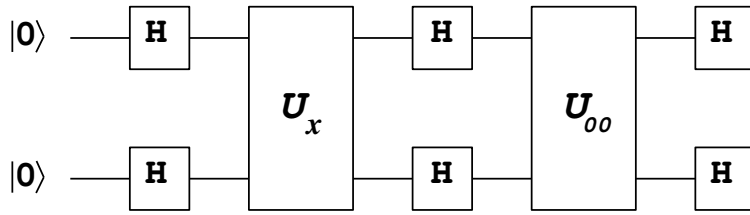
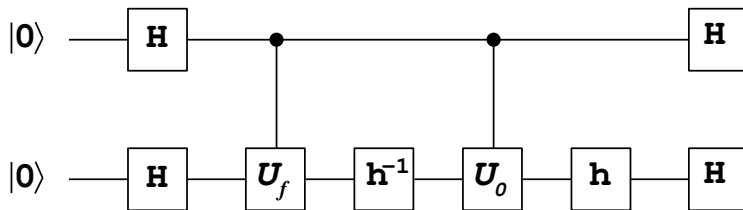


Figure 2

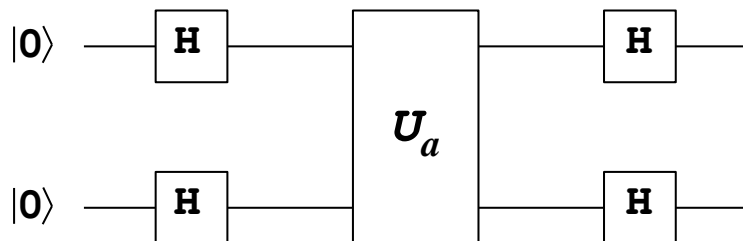
Grover's search algorithm



Approximate quantum counting



Berstein-Vazirani problem



(d) Hogg's algorithm

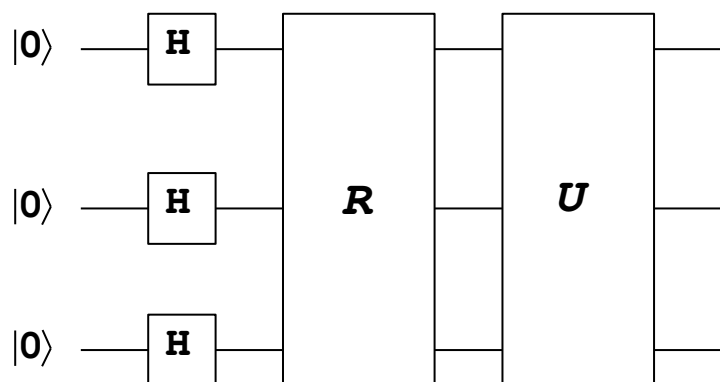


Figure 3

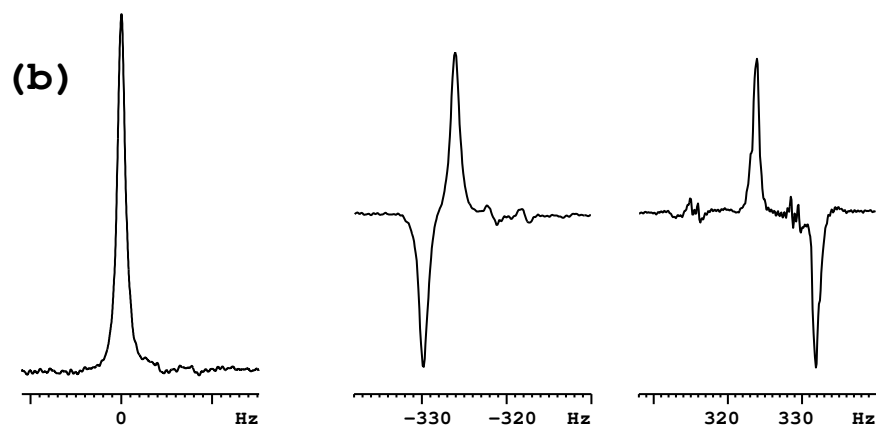
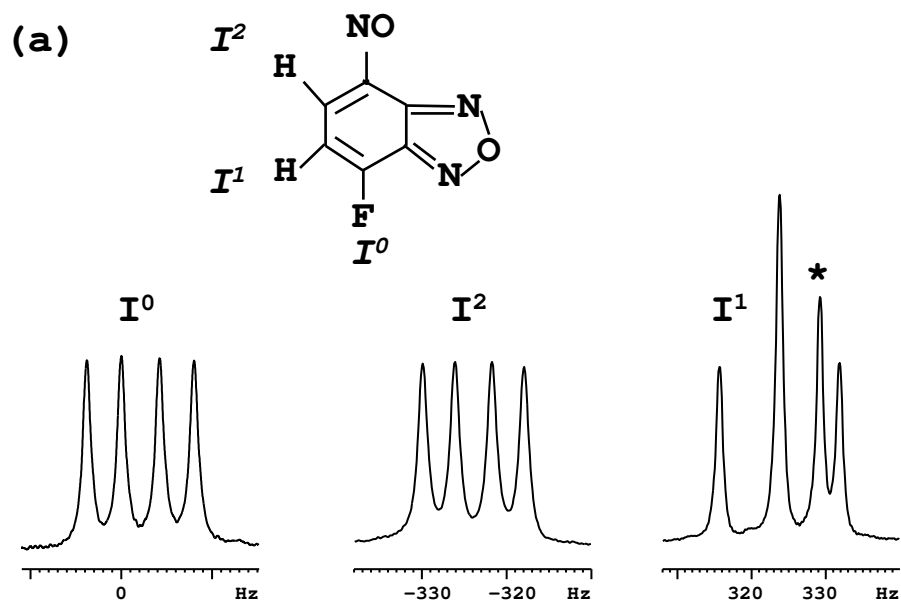
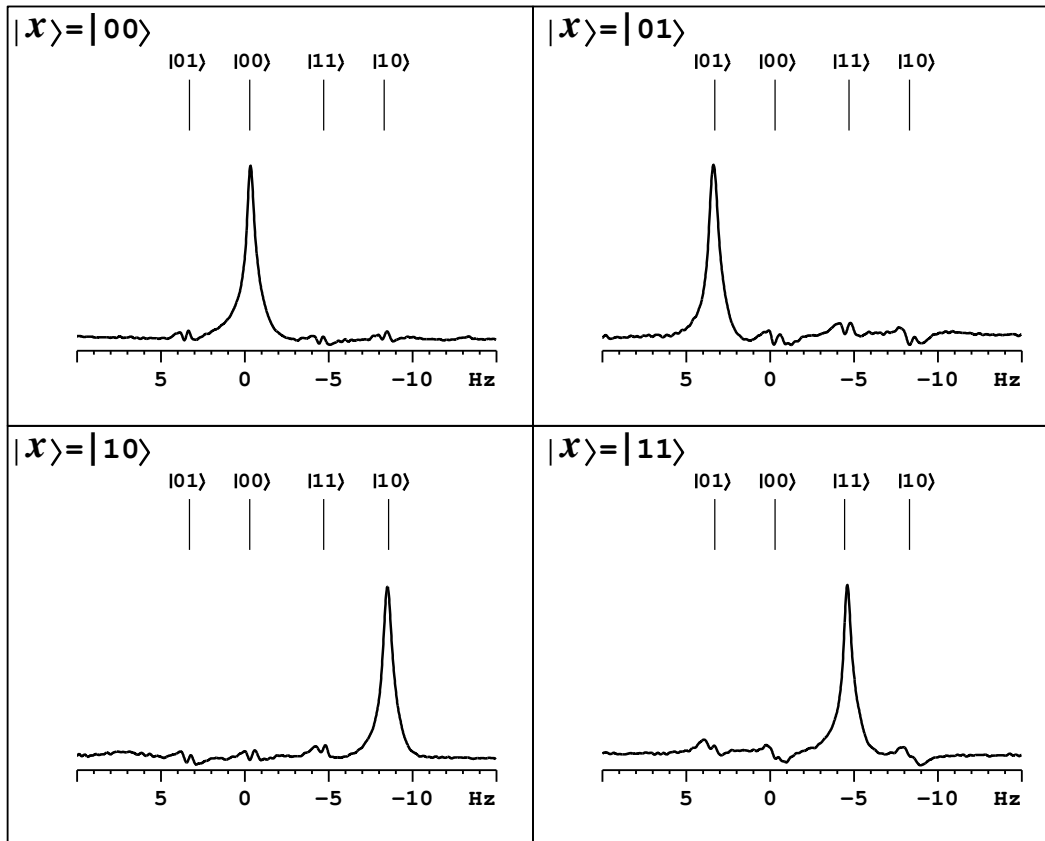


Figure 4

(a)



(b)

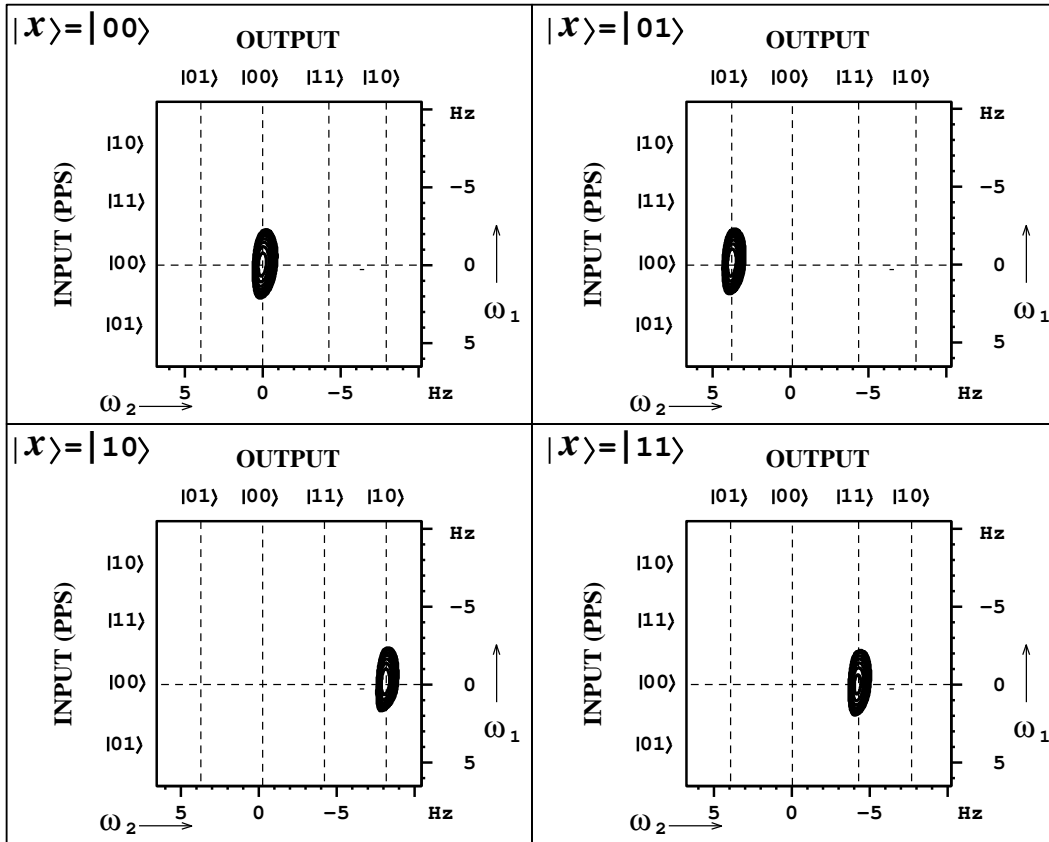
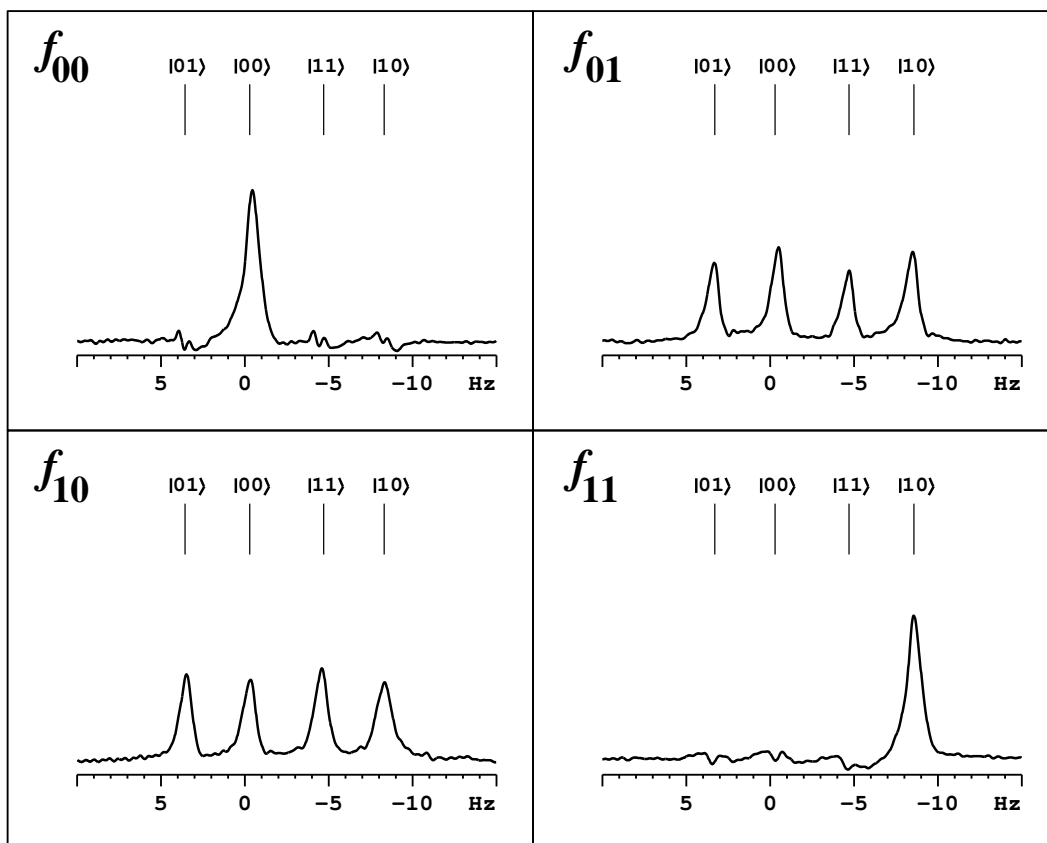


Figure 5

(a)



(b)

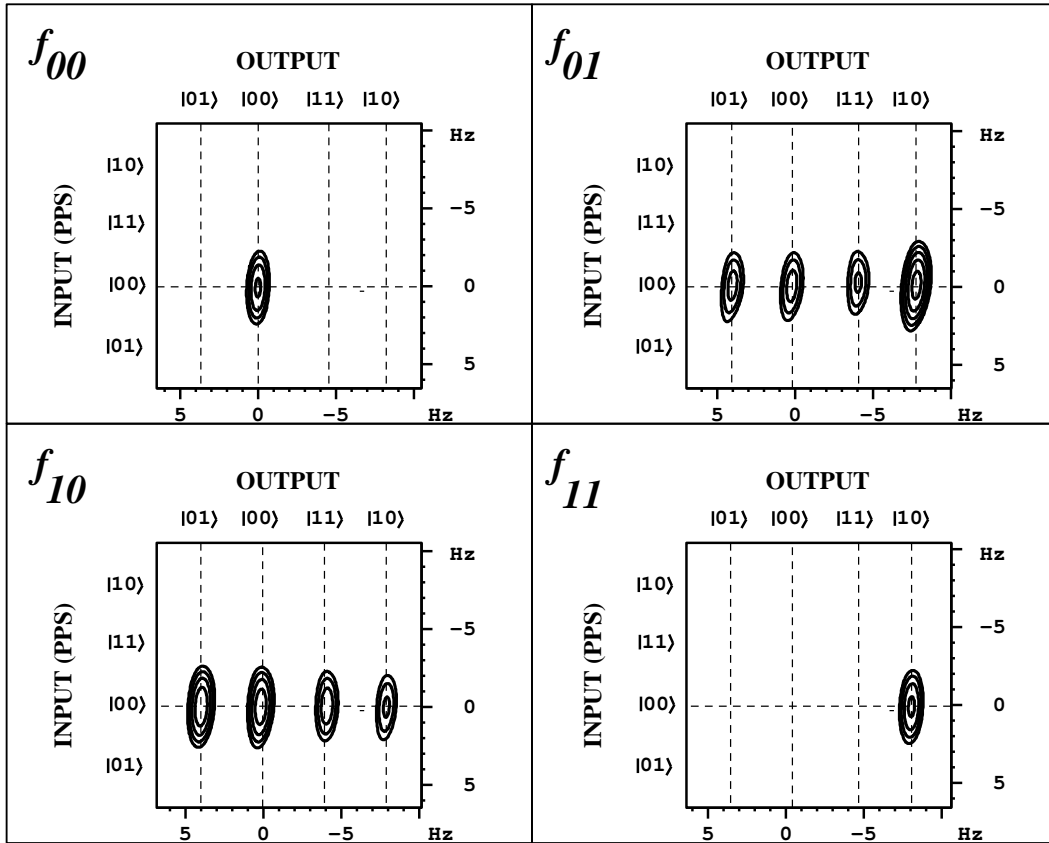
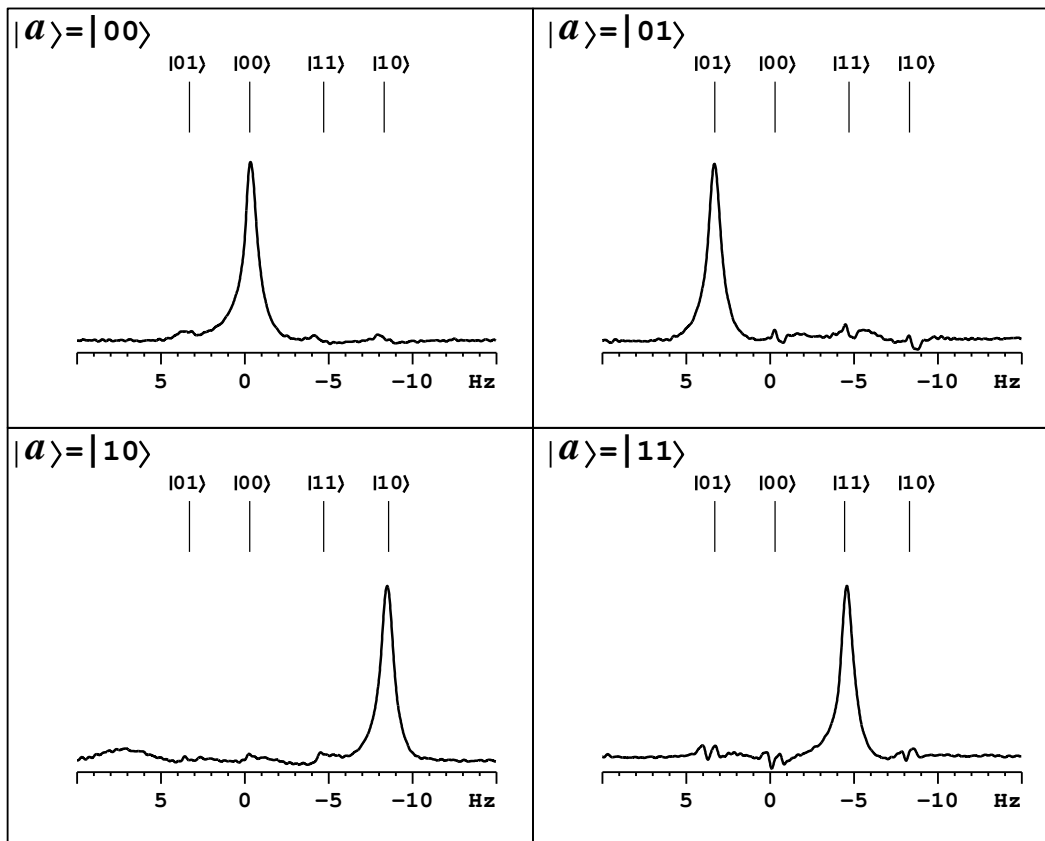


Figure 6

(a)



(b)

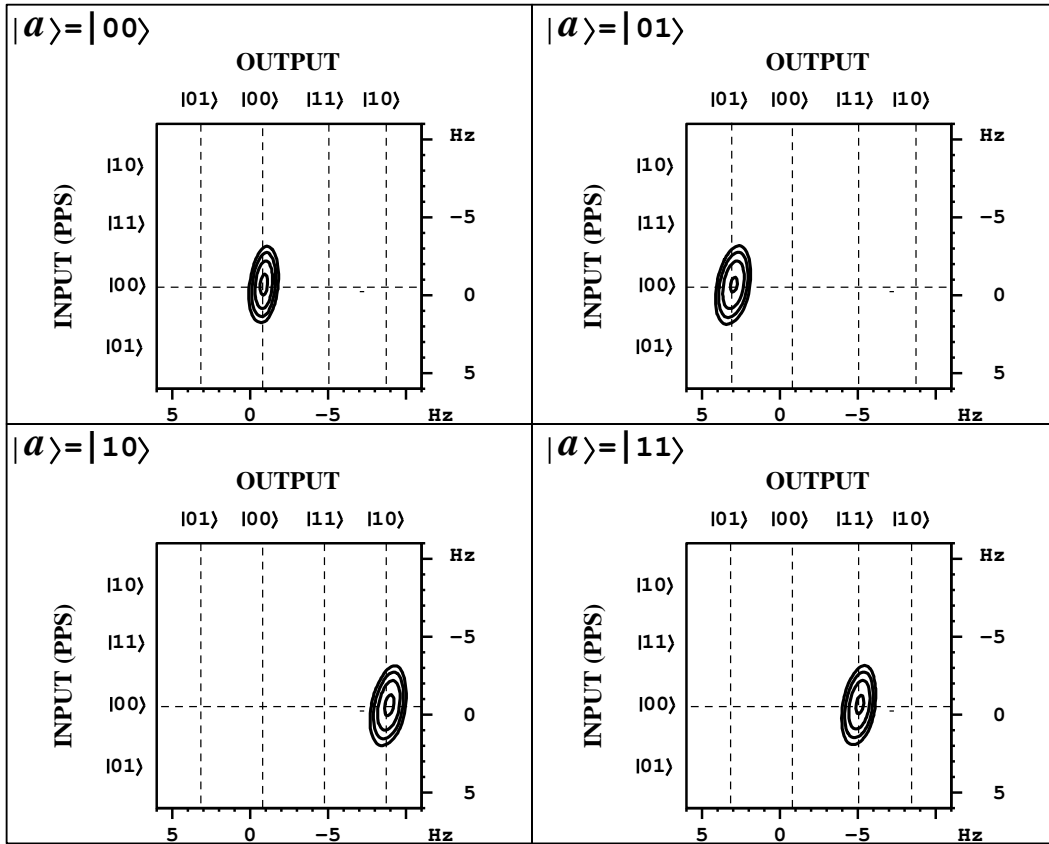


Figure 7

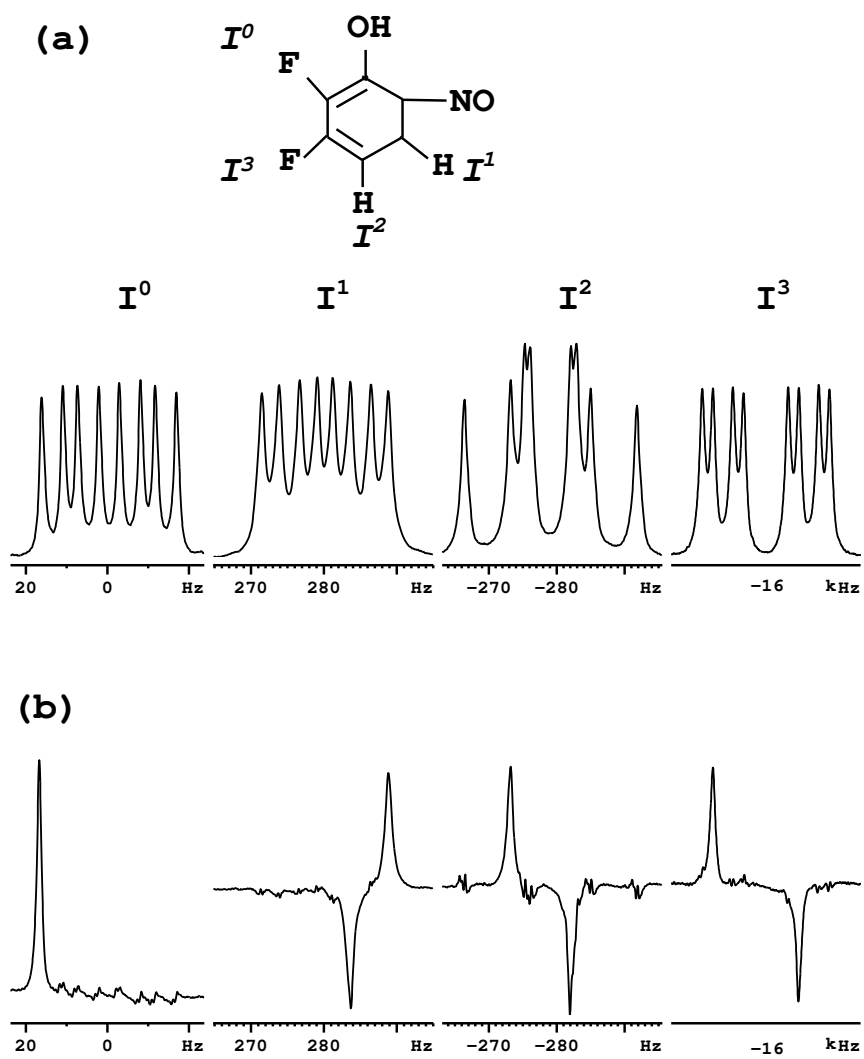


Figure 8

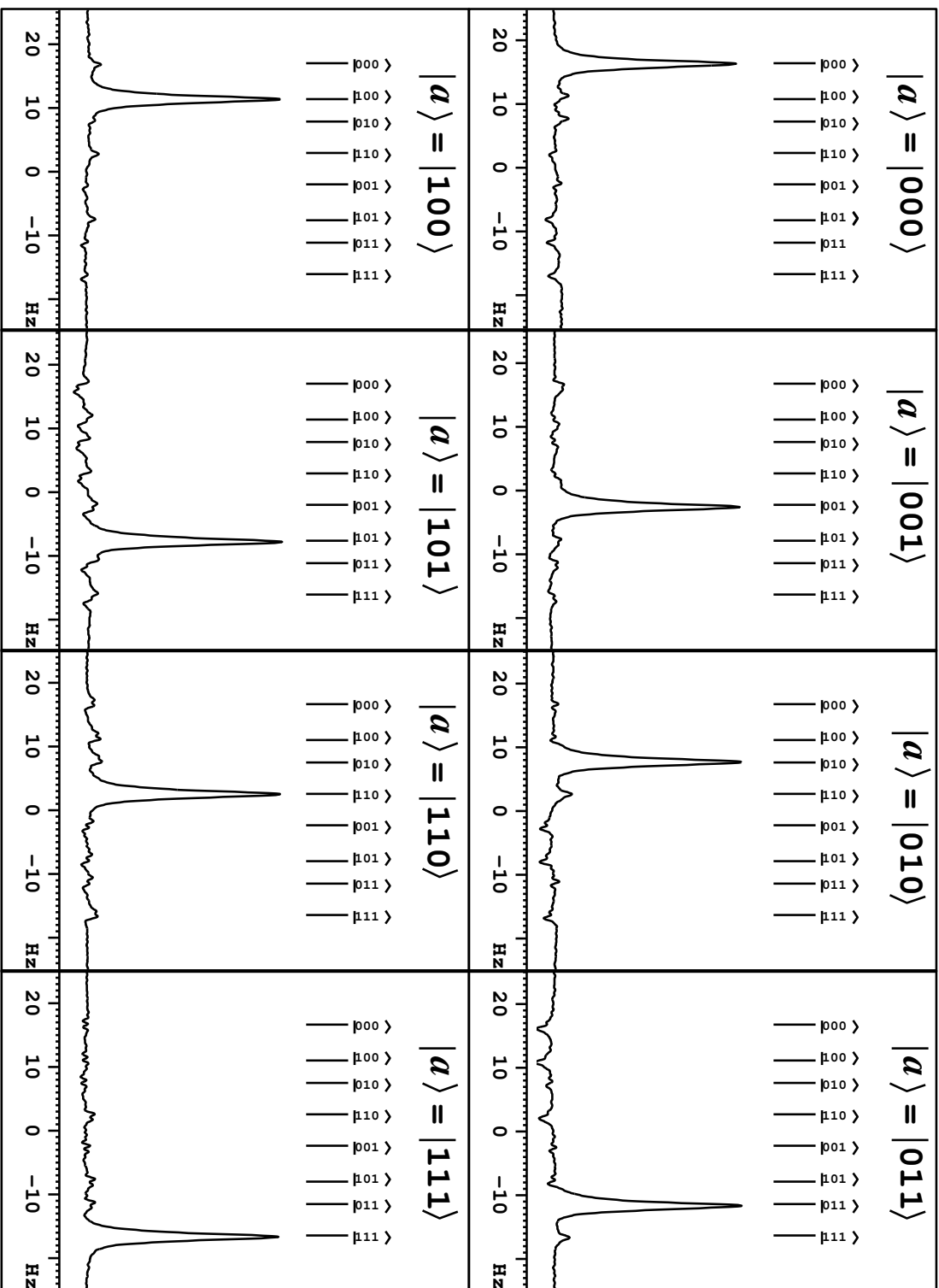


Figure 9(a)

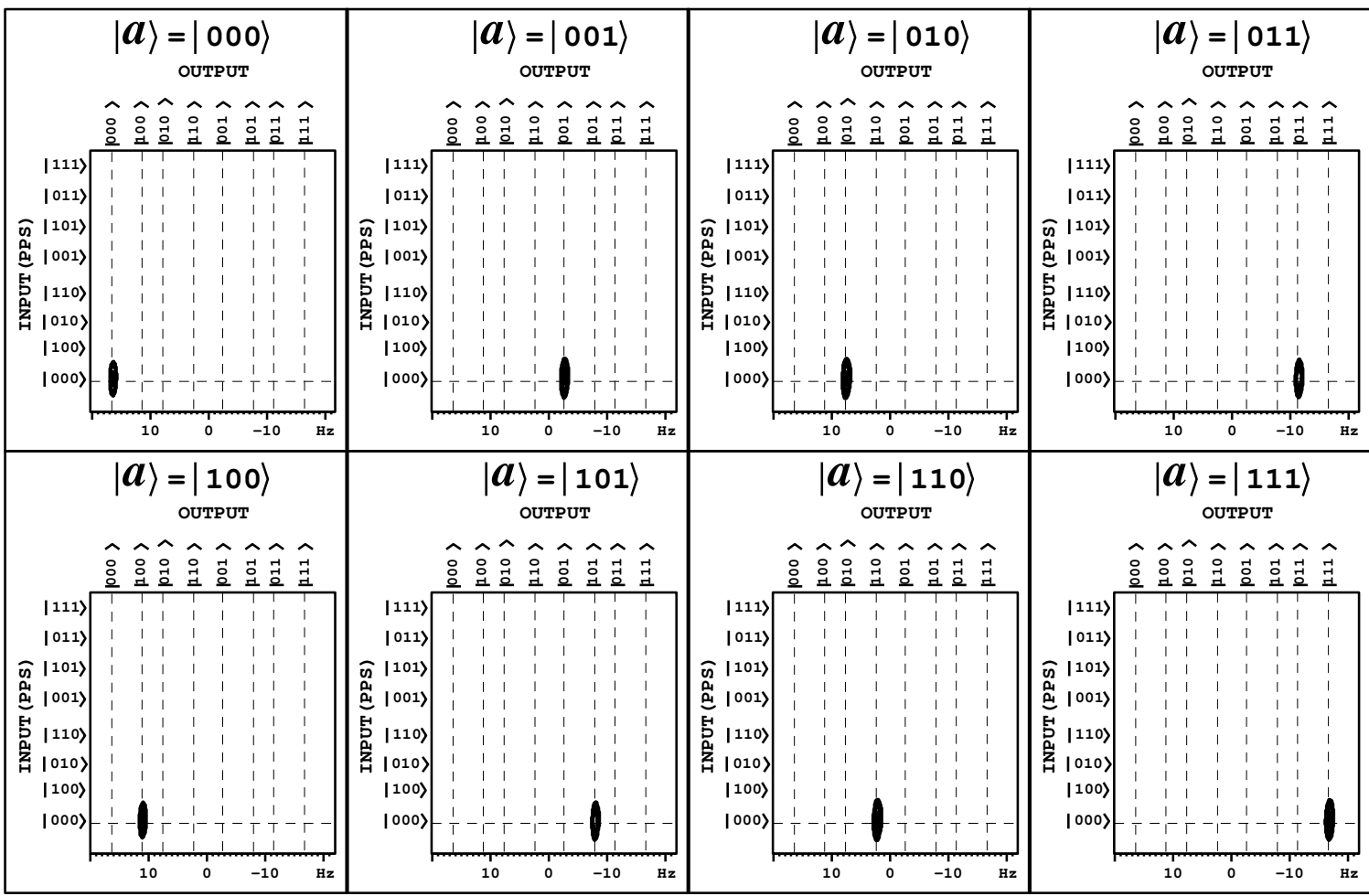


Figure 9(b)

Figure 10(a)

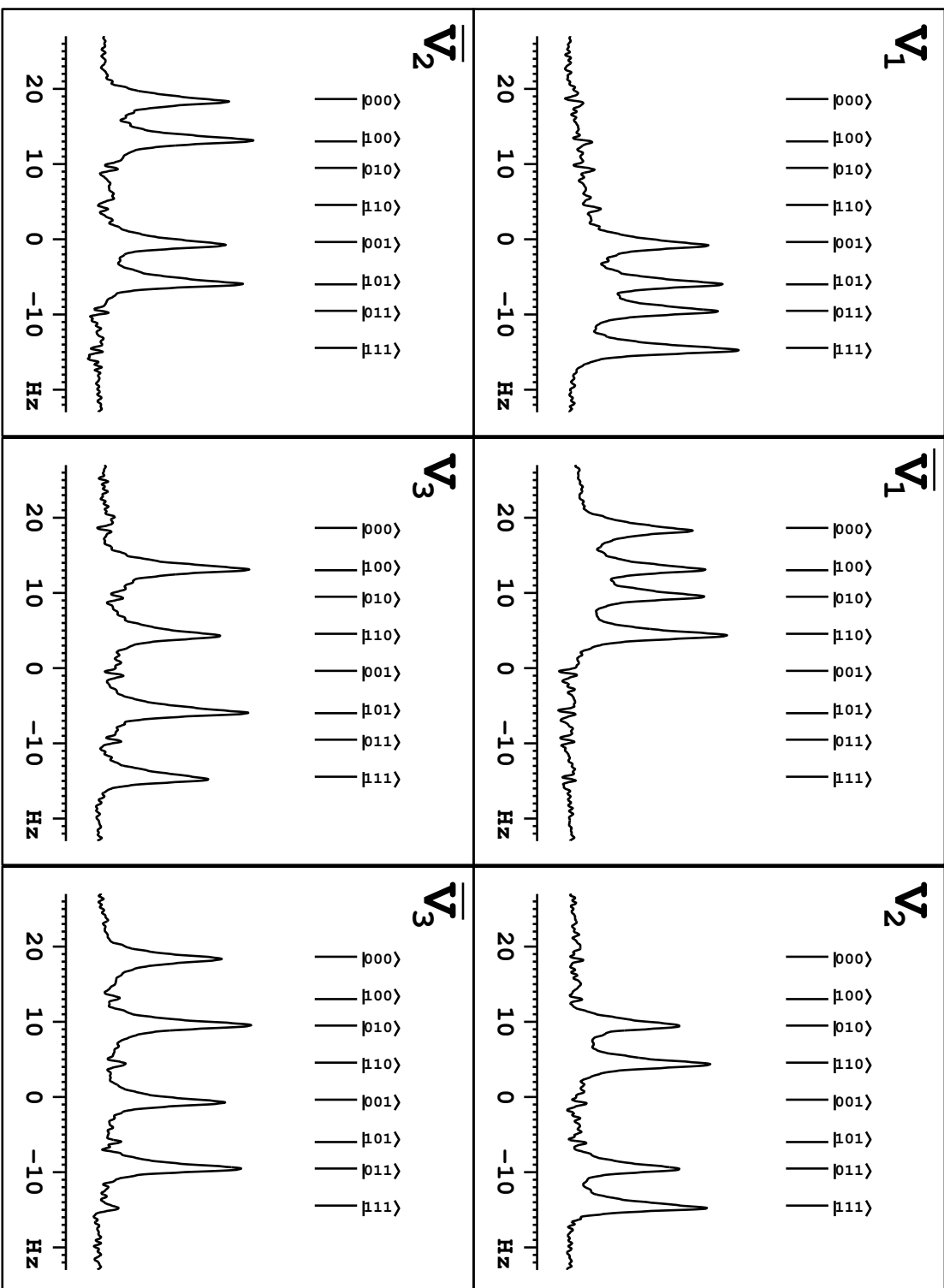
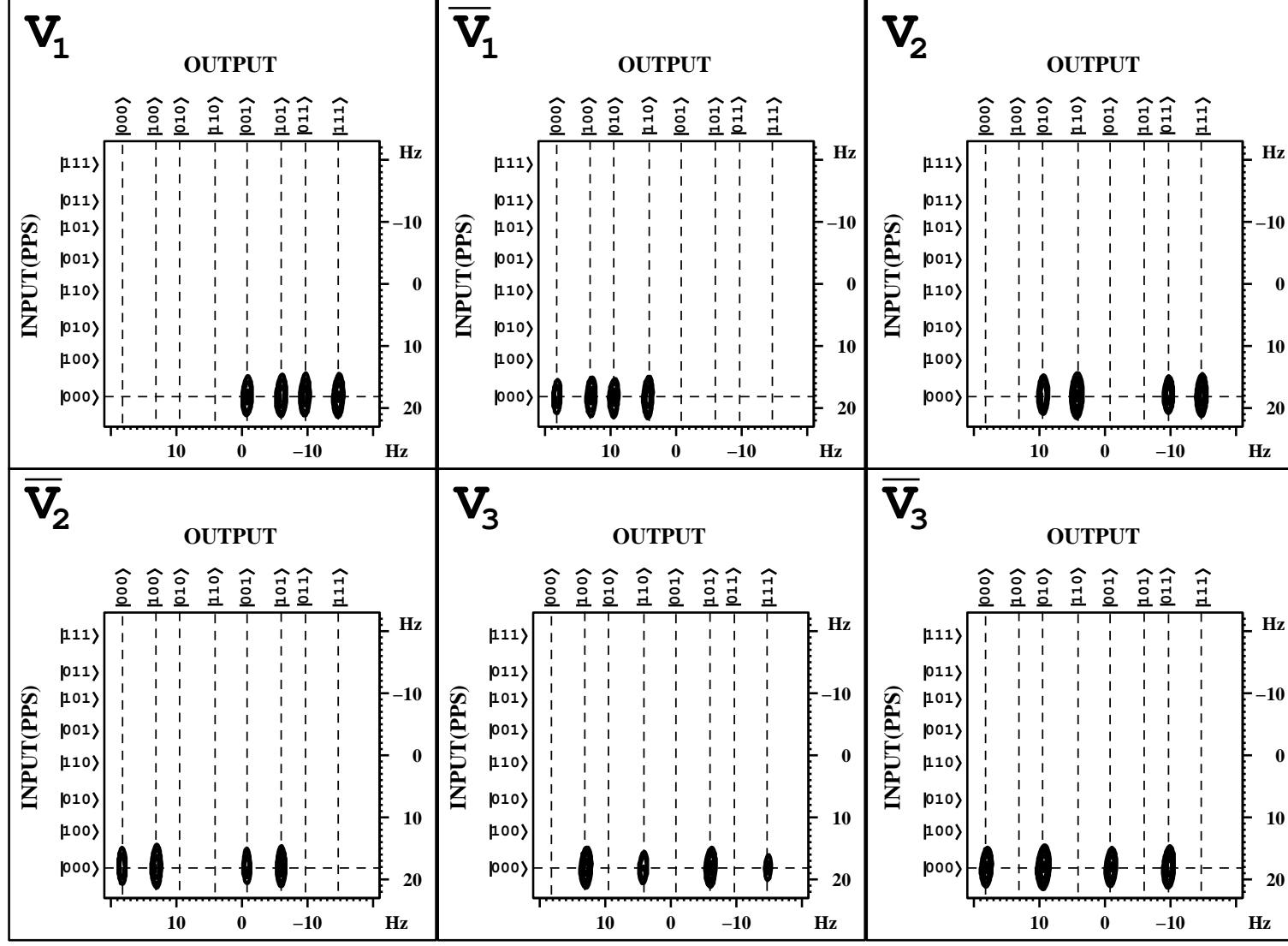


Figure 11(a)



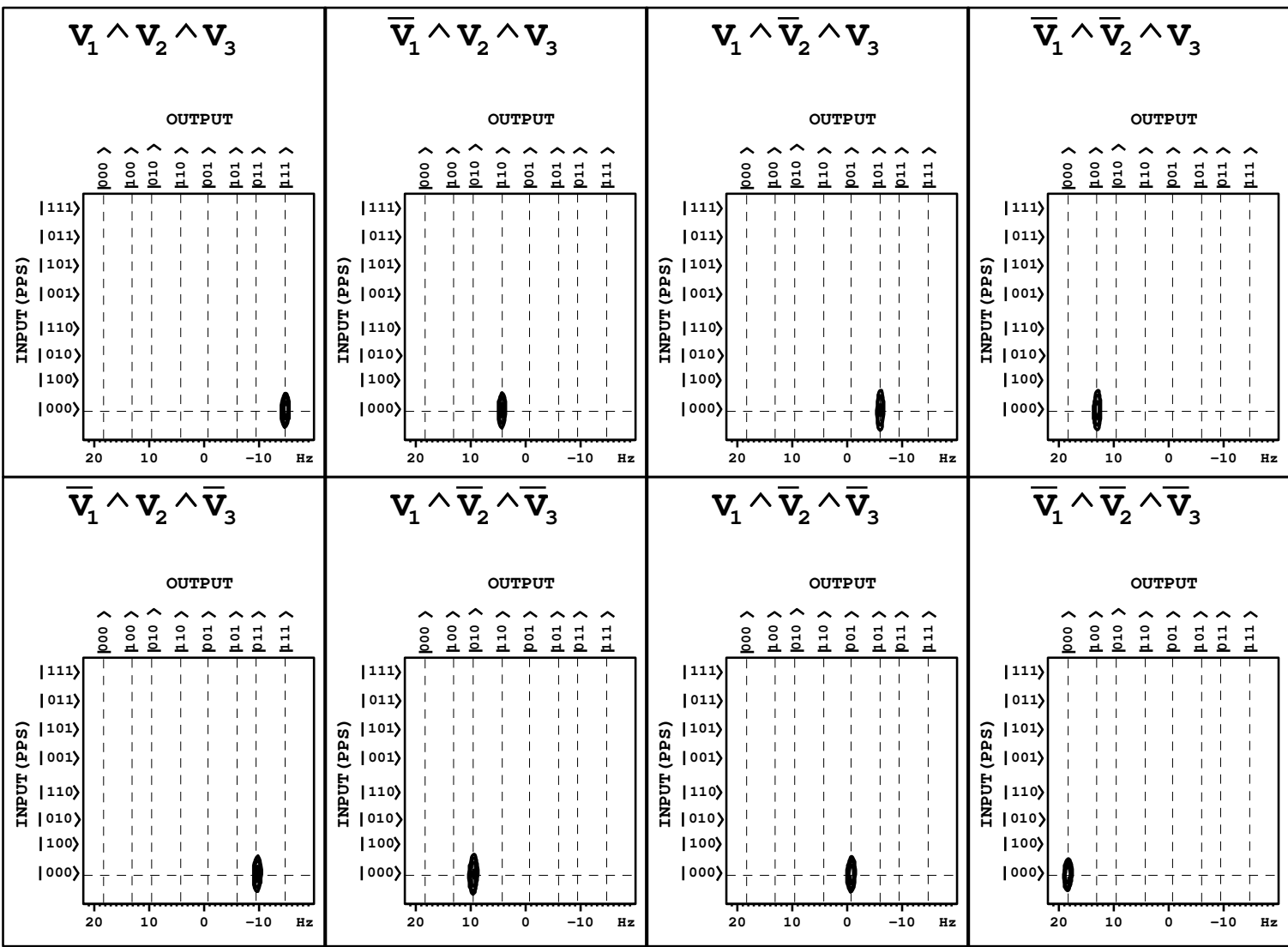


Figure 11(b)